Macromolecules

Article

Cite This: Macromolecules XXXX, XXX, XXX−XXX

Evolution of the Nanoporous Structure of High-Density Polyethylene during Drawing in Supercritical Carbon Dioxide

Anna O. Dudnik,*[,†] Elena S. Trofimchuk,[†] Aleksandr V. Efimov,[†] Nina I. Nikonorova,[†] Ekaterina G. Rukhlya,[†] Lev N. Nikitin,[‡] Igor V. Yaminsky,[†] and Aleksandr L. Volynskii[†]

[†]Lomonosov Moscow State University, GSP-1, Leninskie Gory, Moscow 119991, Russia

[‡]A.N. Nesmeyanov Institute of Organoelement Compounds, Russian Academy of Sciences, 28, Vavilova str., Moscow 119991, Russia

ABSTRACT: The process of open-porous structure development in high-density polyethylene (HDPE) films during uniaxial deformation in supercritical carbon dioxide (SC-CO_2) fluid at 35 °C and 10 MPa has been studied and visualized by means of atomic force microscopy. We suggest that the supercritical fluid act as adsorption-active medium, and the porous structure is developed via the crazing mechanism due to the increasing the distance between of lamellae and the formation of oriented separate fibrils in the intercrystallite space. Effective bulk porosity of the films has been up to 40%. Small-angle X-ray scattering studies and ethanol permeability measurements have revealed that the pores and fibrils are about 10 nm in diameter. The prepared nanoporous materials exhibit good vapor permeability. Structural and mechanical behavior of the prepared porous films has been investigated. Large reversible deformation (up to 80%) of HDPE in the SC-CO_2 has been observed. Repeated drawing of the shrunk films in air under ambient conditions has led to the open-porous structure recovery.

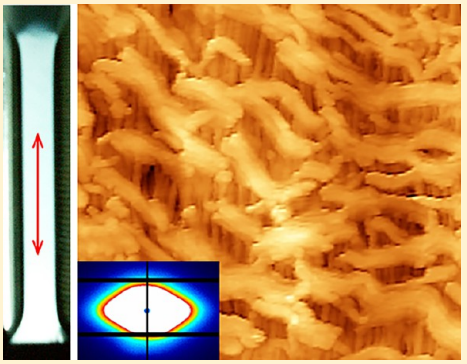

1. INTRODUCTION

Porous polymer materials are widely used as membranes for filtration, reverse osmosis, dialysis, gas separation, controlled release of volatile substances (including drugs), preparation of "breathing" materials, and so forth.[1,2] Moreover, they can serve as a matrix for the preparation of nanostructured materials[3−5] and porous ceramics.[6,7] The development of membrane technology is currently focused on the creation of mechanically, chemically, and thermally stable materials resistant to pollution as well as their cost reduction and durability improvement.

Membranes based on polyolefins (mainly polyethylene PE or polypropylene PP) have been recognized for excellent chemical resistance, good mechanical strength, and low cost. The following methods of porous membranes preparation have been developed:[8−12] (1) sintering of highly disperse polymer powders or fibers, (2) molding from a melt or solution accompanied by the phase separation, (3) irradiation of a polymer film with high-energy particles, (4) etching or leaching the filler phase, (5) foaming, (6) uniaxial or biaxial orientation drawing, and (7) during the synthesis. Undoubtedly, each of the mentioned approaches has its own advantages and drawbacks as well as limitations regarding the characteristics of the obtained porous materials (bulk porosity, morphology, and pore size and size distribution).

Porous membranes with the pores size below 100 nm are the most important, since they are used in ultrafiltration to separate off colloid admixtures, bacteria, and viruses. The applications of such membranes include the preparation of high-purity water in semiconductor, pharmaceutical, and food industries as well as the waste recycling. The membranes are usually produced via the wet spinning, molding methods based on phase inversion or irradiation of a polymer film with high-energy particles followed by etching (the tracking membranes). However, in the case of polyolefins, the preparation of nanoporous membranes using these approaches is complicated and requires special conditions. For example, phase separation is carried out at temperature above the polymer melting point with subsequent cooling (thermally induced phase separation).[13] Preparation of tracking membranes from polyolefins involves the use of solutions of strong oxidizers[14] like chromium(VI) compounds as the etching agent. It should be noted that the average diameter of the pores in the so-prepared membranes is usually of 100−400 nm.

Uniaxial or biaxial drawings are the most widely used for the formation of porous structure in partially crystalline polymers.[15] The deformation approaches can be divided in two groups. Methods of the first groups involve the formation of a hard-elastic structure in the polymer material, via the polymer extrusion under conditions of stretching stress applied to the melt, followed by rapid cooling and annealing at temperature slightly below the melting point.[16] In this case, highly ordered and oriented crystalline structure is formed, consisting of a system of relatively lengthy folded crystals (lamellae) arranged in parallel to each other and perpendicular to the melt flow direction. At the second stage, uniaxial drawing of such hard-elastic materials affords the formation of porous structure. The

Received: October 9, 2017
Revised: December 31, 2017

DOI: 10.1021/acs.macromol.7b02177
Macromolecules XXXX, XXX, XXX−XXX

formed pores are slits with width from tens to hundreds of nanometers; their size and amount depend on the properties of the polymer and the deformation conditions.[17] The second group of methods involves the introduction of a solid particulate filler in a polymer matrix.[18] The pores are then formed during stretching of the filled polymeric samples due to the peeling of the solid particles.[19]

Crazing in a liquid medium is a more universal approach to prepare nanoporous materials based on a wide range of solid amorphous glassy and partially crystalline polymers.[20] According to IUPAC definition,[21] crazing is a formation of cavities containing load-bearing fibrils spanning the gap between the surfaces of each cavity, when a polymer is stressed. The highly disperse fibrillar-porous structure formed during crazing typically contains pores and fibrils with average diameter of 5−30 nm.[22] There are not special requirements for the structure of the polymer subject to crazing.

The crazing process is significantly facilitated in the presence of liquids exhibiting adsorption-active properties with respect to the polymer.[23] Organic solvents (for example, hydrocarbons, alcohols, amines, and so forth) which are toxic, flammable, and explosive substances requiring recuperation are typically used as the adsorption-active media (AAM). Another drawback of crazing in a liquid medium for the preparation of nanoporous polymeric membranes is the required stage of removal of the liquid medium from the pores, leading to the significant structural rearrangements and the decrease in porosity due to the action of the capillary forces.[20,24] These undesirable processes can be avoided using special methods of the liquid removal (such as freeze-drying[25]) or isothermal annealing.[26]

A possible decision to minimize structural rearrangements during removal of the medium from the pores of the polymer obtained via crazing is the use of gaseous AAM. The study of deformation behavior of isotactic PP in the presence of various gases (He, N_2, O_2, CO_2) at pressure of 0.1 MPa over a wide temperature range of −196 to 60 °C has revealed that the gases efficiency as the medium for crazing is the highest at the temperature close to the condensation or sublimation point.[27] Two mechanisms of the gas action during crazing have been suggested: (1) reduction of the interphase energy of the fibrils due to the gas adsorption and (2) facilitation of the plastic deformation of the polymer due to plasticizing action of the gas at the tip of the growing craze. The temperature increase has resulted in the decrease in the amount of the adsorbed gas and, hence, has reduced its crazing action. Other reports[28,29] have marked that the crazing is not observed when the relative gas pressure is below the threshold value of p/p_s = 0.2−0.25. It has been demonstrated that the threshold gas pressure corresponds to the appearance of the gas monolayer adsorbed on the planar surface. The fastest growth of the crazes has been observed at pressure of p/p_s = 0.6−0.8, corresponding to the formation of several molecular layers of the gas at the surface. It has been suggested that the adsorption action of the gas requires its condensation in the forming pores, that is, the appearance of the liquid phase. Using the Tomson−Kelvin equation, it has been shown that surface defects at which the gas condensation starts are about 2.2 nm in diameter.[29]

The use of a gas in the supercritical state can enhance its activity as the crazing agent far from the condensation point. It is known that the physicochemical properties of supercritical fluids are significantly changed depending on the temperature and pressure.[30] Supercritical carbon dioxide (SC−CO_2)[31,32] (the critical parameters: T 31.8 °C and p 7.4 MPa), being cheap, nontoxic, nonflammable, and relatively inert, is currently most widely used as a supercritical fluid. It readily evaporates off upon decrease of the pressure in the cell, thus overcoming the issue of the solvent removal. SC-CO_2 is often used for the preparation of porous materials based on different polymers via foaming.[33] The formed pores are usually cellular and closed, their size being of 0.1−10 μm. The concentration of CO_2 dissolved in the polymer is the major factor affecting the parameters of the porous structure. Therefore, the saturation with carbon dioxide is usually carried out at temperature close to the glass transition temperature of the amorphous polymer (poly(methyl methacrylate) PMMA,[34,35] polystyrene PS,[36,37] polycarbonate PC,[38] etc.) or to the melting point of the partially crystalline substrate (PP,[39,40] PE,[41] polylactide PLA,[42] etc.). Uniaxial deformation in the SC-CO_2 has been sometimes used[43,44] to reduce the temperature and time of the polymer exposition in the supercritical fluid, increase the amount of the absorbed gas, and allow better control of the morphology of pores.

Another mechanism of porous structure formation has been earlier described for isotactic PP film stretched in the SC-CO_2 at p 10 MPa and T 35 °C.[45,46] In detail, the formation of noncellular pores with diameter of 10 nm localized in the interlamellar space was observed. Based on the SAXS data and the analysis of mechanical behavior of the porous polymeric films, the crazing mechanism of the nanoporous structure formation has been suggested. Similar results have been described in ref 47.

This study aimed at systematic investigation of specific features of uniaxial deformation of extruded films of partially crystalline high-density polyethylene (HDPE) in the SC-CO_2 and the development of the porous structure. We determined the conditions of the crazes formation and the parameters of the crazes using a set of structural (SAXS, SEM, and AFM) and mechanical methods. Special focus was paid to visualization of the evolution of HDPE structure during deformation by means of AFM. The obtained data can be used to elucidate the mechanism of polymers deformation in supercritical media affording nanoporous polymeric membranes with given properties and to predict the physical and mechanical properties of the materials operating under such specific conditions.

2. EXPERIMENTAL SECTION

Commercial HDPE films (M_w 200 kDa, thickness 75 μm, mp 130 °C, degree of crystallinity 70%, prepared via extrusion blow molding) were studied. The specimens were of dog bone (gage area 6 × 20 mm^2) or rectangular (45 × 30−50 mm^2) shape.

Uniaxial deformation of the polymeric films was performed using a high-pressure stretching device developed at INEOS and MSU (Department of Chemistry). The scheme and image of the device are shown in Figure 1. A specimen was clamped in the stretching device which was placed in a high-pressure cell and equilibrated at 35 ± 0.1 °C for 30 min on a water bath (temperature was maintained constant using a temperature controller IKA). The cell was then filled with CO_2 (purity 99%), pressurized to a predefined level (10−30 MPa, pressure adjustment accuracy ±1 MPa), and equilibrated for 10 min. The specimen was then stretched along the machine direction to the demanded relative deformation (50−400%) that was calculated as follows:

$$\varepsilon = \frac{l_1 - l_0}{l_0} \times 100$$

with l_0 being the initial specimen length and l_1 being the stretched specimen length. The drawing rate was of 25%/min. CO_2 was

DOI: 10.1021/acs.macromol.7b02177
Macromolecules XXXX, XXX, XXX−XXX

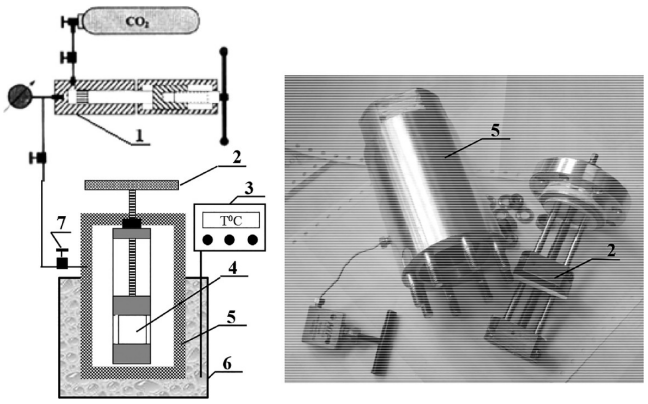

Figure 1. Scheme (left) and image (right) of the high-pressure cell for uniaxial deformation of a polymer film in supercritical fluid: 1, pressure generating gun; 2, stretching device; 3, temperature indicator; 4, specimen; 5, high-pressure cell; 6, water bath; 7, inlet/outlet valve.

removed from the cell at the highest possible flow rate (about 6 mL/s). The drafting device was then taken off the cell, and the polymeric specimen was fixed using special clamping frames.

To investigate the effect of reversible deformation, some of the samples were first stretched in the SC-CO_2 to certain relative deformation and then relieved to the initial length by rotating the knob of the drafting device in the reverse direction. Then the specimen was taken out of the cell and left for relaxation for 48 h at atmospheric pressure. The relative shrinkage (α, %) was expressed as the ratio of the reversible deformation and the relative deformation at the stretching stage:

$$\alpha = \frac{l_1 - l_2}{l_1 - l_0} \times 100$$

with l_0 being the initial specimen length, l_1 being the stretched specimen length, and l_2 being the specimen length after longitudinal shrinkage.

The specimens' appearance was documented using a Sony digital camera or Carl Zeiss polarized light microscope (Jena) in the transmission or reflection mode with 100× magnification.

The deformed specimens were characterized by the volume increase (dV/V_0, vol %) and effective bulk porosity (W, vol %) calculated as follows:

$$\frac{dV}{V_0} = \frac{V_1 - V_0}{V_0} \times 100$$

and

$$W = \frac{V_1 - V_0}{V_1} \times 100$$

with V_0 and V_1 being the initial specimen volume and its volume after the deformation in SC-CO_2, respectively. The specimen volume was calculated from its dimensions determined at atmospheric pressure after taking the specimen out of the high-pressure cell.

Porous structure of the deformed polymeric film was studied by means of liquid permeability under the pressure gradient using an FMO-2 ultrafiltration cell under conditions preventing the specimen shrinkage. Ethanol at 0.2 MPa overpressure was used as the test liquid. The average pore size ($\bar{D}_{pore}$, nm) was calculated using the Poiseuille equation:

$$\bar{D}_{pore} = \sqrt{\frac{8\eta h G}{W \Delta P}}$$

with η being the liquid viscosity, h being the specimen thickness, G being the liquid flow through the specimen, W being the effective bulk porosity, and ΔP being the pressure gradient.

Vapor permeability was determined using a cell developed at MSU (Department of Bioengineering and Bioinformatics); see the scheme and image in Figure 2.

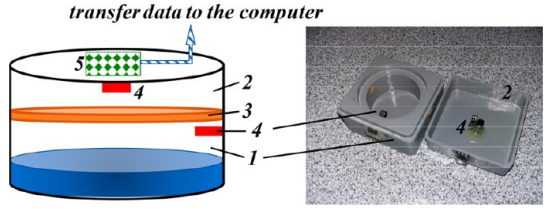

Figure 2. Scheme (left) and image (right) of the cell for vapor permeability measurement: 1, vessel with water; 2, sealed cap; 3, specimen; 4, humidity and temperature sensors; 5, Arduino Nano microprocessor plate.

The cell case was manufactured of ABS plastic using a Maker Bot replicator 2X 3D printer. The measuring cell was put in a thermostat maintaining temperature constant at 25 °C. The humidity was measured using an HIH-4000-004 Humidity Sensors analogue device. The data (humidity and temperature) acquisition and processing were performed using an Atmega 328 microcontroller integrated in the Arduino Nano microprocessor plate, and the processed data were transferred to PLX-DAQ software. Each point in the relative humidity (RH) plots was averaged from 100 readings per second taking into account temperature fluctuations. Average humidity in the measuring cell in the absence of the liquid was of 30%, and that over saturated water vapor was of 95−100%.

Mechanical tests of the polymer specimens (the dog-bone shape with the gage size 6 × 20 mm^2) were performed at room conditions (22−24 °C and 0.1 MPa) using an Instron-4301 tensile testing machine at the constant drawing rate of 50%/min.

Structures of the initial and deformed samples were used by means of WAXS and SAXS. To do so, the specimens were fixed in special clamps at given tensile strain. WAXS patterns were obtained using the "Belok" Station at Kurchatov Centre of Synchrotron Radiation (Moscow, Russia) (beamline 4.4e of Kurchatov Synchrotron radiation source) equipped with a Rayonix SX165 detector operating at a resolution of 2048 × 2048 pixels (pixel size was 80 μm). The sample-to-detector distance was 150 mm. The synchrotron radiation wavelength was 0.0987 nm.

SAXS measurements were performed at DIKSI beamline of Kurchatov Centre of Synchrotron Radiation (Moscow, Russia). The synchrotron radiation wavelength was 0.16 nm, and the vacuum chamber length was 2.4 m, allowing SAXS patterns measurements in the scattering vector (q) range of 0.07−1.1 nm^{-1}. The vector was calculated as follows:

$$q = \frac{4\pi \sin(\theta)}{\lambda}$$

where θ is the Bragg angle and λ is the radiation wavelength. The q range was calibrated using silver behenate as the standard sample. The scattering was measured with Dectris Pilatus3R 1M detector at 300 s exposition and then processed using Fit2D software to obtain the 1D scattering intensity profile as a function of scattering vector module, $I(q)$. The pixel size in the scattering pattern was 172 μm. The average size of the fibrils was calculated from the SAXS data as described elsewhere.[46]

Morphology of the surface and bulk of the polymeric samples was studied by means of SEM using a CamScan-S2 microscope (accelerating voltage 20 kV) and a Hitachi TM3000 microscope (accelerating voltage 15 kV). The deformed film was fixed in a special clamp to avoid its shrinkage and the collapse of the porous structure. The specimens for SEM observation of the bulk of the deformed films were prepared by cooling with liquid nitrogen and fractured along the deformation direction. The specimen cleavage was left fixed in the clamping device. The fixed samples were attached to the surface of a special microscope table with conducting carbon double-sided sticky

DOI: 10.1021/acs.macromol.7b02177
Macromolecules XXXX, XXX, XXX−XXX

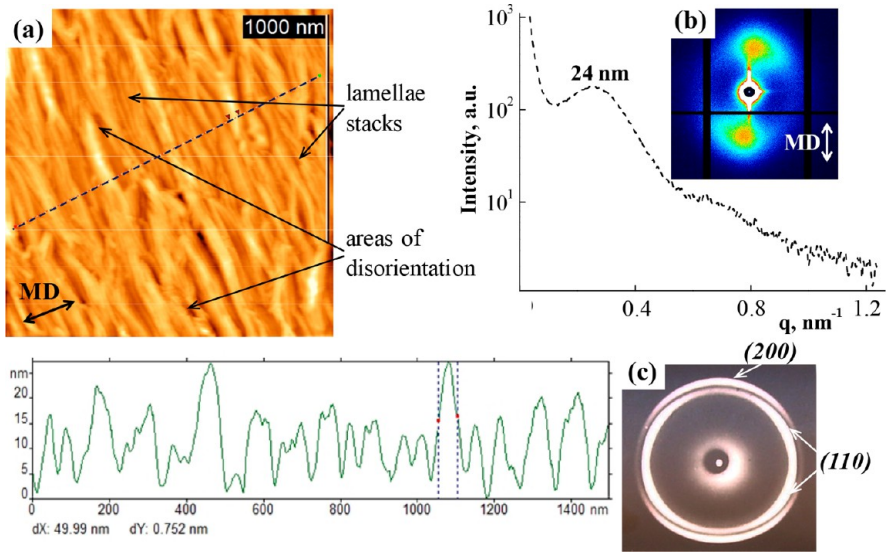

Figure 3. AFM image and the cross section along the selected direction (a), SAXS (b), and WAXS (c) patterns of the initial HDPE film.

tape, and a gold layer with a thickness of 50−70 nm was sprayed onto them with a Giko IB-3 setup by the method of ionic plasma sputtering in the presence of Ar (p 0.1 Torr) at 6 mA for 5 min.

AFM studies were performed in the contact mode using a Solver PRO-M atomic force microscope. With the help of this method the structure of the initial, deformed and shrunk HDPE films was studied. The deformed HDPE films were fixed by their contour in the metallic frameworks to prevent shrinkage and the collapse of the porous structure. The observations were performed in water to avoid the effect of the capillary force between the specimen and the cantilever probe. Water does not wet the hydrophobic HDPE surface and does not penetrate into the pores. Moreover, water is safe and evaporates relatively slowly at room temperature. A PNP-DB chip with rectangular cantilevers (100 and 200 μm long, with rigidity of 0.48 and 0.06 N/m, respectively) was used as the contact probe. AFM images were processed and analyzed using FemtoScan Online software (Advanced Technologies Center, Russia).[48] The average distances between the centers of the lamellae stacks (L) and the average spacing between the fibrils centers (d) were determined from AFM images. Each value of L or d was averaged as a result of 300 measurements.

3. RESULTS AND DISCUSSION

3.1. Deformation of HDPE Film in Air. To begin with, the structure of an initial industrial film and its mechanical behavior during uniaxial deformation in air at 0.1 MPa and 35 °C are studied. We used HDPE film prepared via the melt extrusion blow molding, that is, under conditions of the polymer crystallization under stress. The structure of similar films has been described earlier in refs 49−51. Under the mentioned conditions, the growing lamellae formed spirals oriented in the transverse direction, the spiral axis being parallel to the b-axis of the crystal and the a-axis being predominantly parallel to the machine direction, the structure corresponding to the so-called a-texture.

Figure 3 shows the AFM image (a) along with small-angle (b) and wide-angle (c) scattering patterns for the initial HDPE film. It is to be seen that the lamellae in the nondeformed film (white threads in the image) are mainly oriented perpendicular to the machine direction. However, the areas showing significant disordering of the lamellae are observed in the film. The height profile (Figure 3, bottom left) along the dashed line drawn perpendicular to the major axis of the lamellae revealed the presence of the lamellae stacks with average thickness of 40−50 nm. Certain magnified images showed the presence of isolates lamellae with thickness about 15−20 nm.

The SAXS pattern contained strong drop-shaped reflections on the meridian and a weaker annular reflection. Such pattern shape is typical of extruded HDPE film, evidencing the predominant orientation of the lamellae planes (major axis of the lamellae) perpendicular to the extrusion direction. Using the SAXS data, the large period for the HDPE film was calculated ($L = 2\pi/q_{max}$); for the reflections on the meridian, $q_{max} = 0.26$ nm^{-1} and $L \approx 24$ nm.

The WAXS pattern contained the (200) reflection as two arcs on the meridian and the (110) reflection as four off-meridian arcs. According to the reference data,[52] such a pattern is typical of the lamellae twisting about the b-axis, the latter being perpendicular to the machine direction.

Uniaxial stretching of the HDPE film in air occurred via the neck formation. Figure 4 shows the stress−strain curves

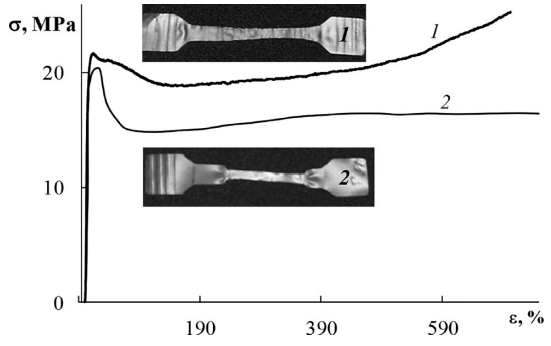

Figure 4. Stress−strain curves for the deformation along (1) and perpendicular (2) to the machine direction of the initial HDPE film and the appearance of the specimens deformed by 150%.

obtained during the deformation along and perpendicular to the machine direction along with the appearance of the samples after the drawing by 150%. It is clearly seen that the curves are somewhat different, typical of the films with the a-texture. The yield stresses in the two experiments were close, of 21−22 MPa. The specimens' appearance evidenced the uniaxial

DOI: 10.1021/acs.macromol.7b02177
Macromolecules XXXX, XXX, XXX−XXX

deformation via the neck formation in both directions. However, the neck formed during stretching in the longitudinal direction was relatively wide and less pronounced due to the presence of the areas with the lamellae ordered perpendicular to the machine direction. That effect could result from a combination of two deformation mechanisms: shear and separation of the lamellae to form the crazes. On the contrary, the deformation in the transverse direction occurred mainly via shear mechanism, and the neck revealed conventional shape with distinct local narrowing of the working part of the sample.

Further experiments were limited to the study of mechanical behavior of the HDPE film and its structure evolution during the deformation along the machine direction. Figure 5 displays

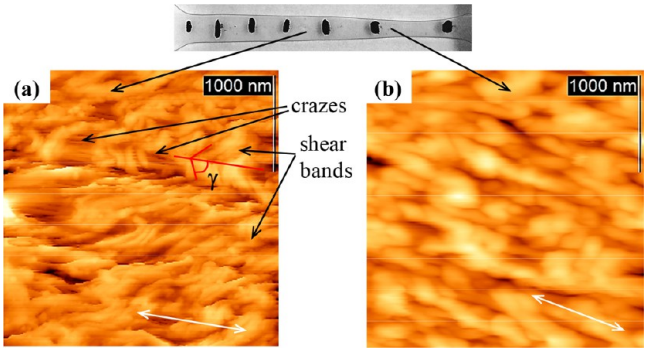

Figure 5. Appearance of the polymeric sample after drawing in air along the machine direction to 100%. AFM images of two parts of the stretched HDPE film surface with the local relative deformation of 110% (a) and 290% (b). Arrows mark the deformation direction.

the appearance of the polymeric sample after its deformation in air along the machine direction to the neck formation. The engineering tensile strain of the specimen equaled 100%; to determine the local relative deformation, the marks were put at the specimen gage with 3 mm spacing.

It is to be clearly seen that the uniaxial deformation of the film in air was nonuniform. The distances between the adjacent marks were significantly different, the local relative deformation being 50−290%. AFM images of different pieces of the specimen were obtained: those with the local deformation corresponding to the engineering one (ε = 110%) and to that of the neck (ε = 290%). When the local deformation was relatively low (before the neck formation), the lamellae were bended and twisted with respect to the stretching direction by about γ = 40°−56° (cf. Figure 5) via the shear mechanism. Moreover, single crazes formed due to separation of the lamellae stacks were observed; however, the bulk porosity in that specimen part did not exceed 10%. For the neck with the local deformation reaching 290%, relatively dense structure was observed, consisting of crystallites arranged as beads predominantly oriented along the deformation direction. Such structure was formed due to the fragmentation of the lamellae and their orientation along the stretching direction.

Hence, uniaxial deformation of the HDPE film produced via extrusion blow molding was accompanied by fragmentation of the initially stacked lamellae and transformation of the starting lamellar *a*-texture in the oriented one and resulted in the formation of monolithic nonporous neck.

3.2. Deformation of HDPE Film in SC-CO_2 Fluid. Stretching of the HDPE film along the machine direction in the supercritical carbon dioxide fluid at 10 MPa and 35 °C occurred differently. Under the mentioned conditions, the specimen deformation was uniform without neck formation, and the process was accompanied by whitening of the sample (see the inset in Figure 6). The working part of the stretched specimens

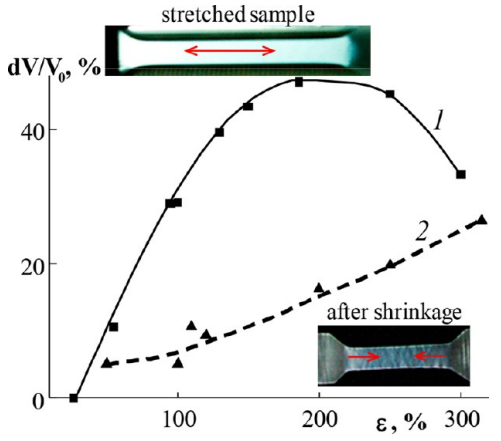

Figure 6. Relative volume increase dV/V_0 of the HDPE film as a function of its relative elongation during deformation in the SC-CO_2 (1) and residual porosity of the specimen after its drawing to ε and shrinkage in the SC-CO_2 (2). The insets show the appearance of the specimen after its drawing to 100% and after the shrinkage.

was slightly narrowed up to high tensile strain. Curve 1 in Figure 6 shows the relative volume increase dV/V_0 of the HDPE specimen as a function of relative elongation in the SC-CO_2. The increase in the volume due to the formation of the porous structure was observed starting from the relative deformation of 20−30%. The increase in the relative deformation to 120−150% resulted in almost linear growth of the dV/V_0 value, whereas further stretching of the sample to ε of 250% was accompanied by slower increase in the volume, the highest porosity value being of 45 vol %. When relative deformation exceeded 250%, the porosity was somewhat lowered.

Curve 2 in Figure 6 shows the residual porosity of the drawn sample after its unloading in the SC-CO_2. The specimen shrinkage (cf. its appearance in the inset in Figure 6) and recovery of its linear dimensions were accompanied by the decrease in the volume of the pores developed during the specimen drawing. The observed significant reversibility of HDPE deformation in the presence of SC-CO_2 will be considered in more detail below. It should be noted that similar features of the volume increase during uniaxial stretching and its decrease upon unloading of polymer sample have been earlier observed for the HDPE crazing-type deformation in different AAM[20,22] (for example, *n*-heptane or isopropanol).

The specimens deformed in the SC-CO_2 could be readily colored with an alcoholic solution of the dye. As an example, optical microscopy images of the specimen drawn by 100% before and after keeping in an ethanolic solution of Rhodamine B for 10−15 s are shown in Figure 7. Even such short exposition to the dye solution was enough for penetration of Rhodamine B in the porous structure of the deformed HDPE, reflected in strong red coloration of the film which simultaneously turned transparent. After the solvent evaporation, the polymeric film became magenta color and nontransparent. The observation evidenced the formation of

DOI: 10.1021/acs.macromol.7b02177
Macromolecules XXXX, XXX, XXX−XXX

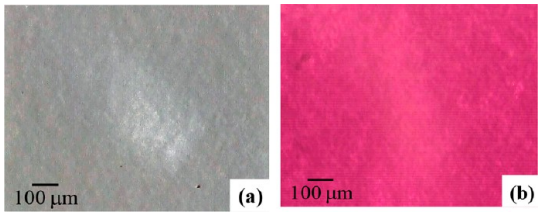

Figure 7. Light microscopy images of the HDPE film stretched by 100% in the SC-CO_2 before (a) and after (b) immersion in ethanolic solution of Rhodamine B.

percolating pores during HDPE deformation in the supercritical fluid.

Important data on the porous structure formed during drawing of HDPE in the SC-CO_2 were obtained by means of the pressure-driven liquid permeability. The results of the study of the HDPE films permeability to ethanol are collected in Table 1. It is to be seen that the films drawn by 80−300% in the SC-CO_2 were permeable to ethanol. The increase in the relative deformation led to steady increase in the flow rate, up to the highest value of 7 L/(h m^2) at the tensile strain of 300%. It should be noted an abrupt increase (by 10 times) of the value of ethanol flow through the film with the growth of the tensile strain from 110% to 220%. That fact could be attributed to the difference of the true pathway of the liquid through the film (the flow route tortuosity). Likely, the connectivity of pores became higher with increase in the relative deformation, and the flow rate of ethanol sharply increased.

Table 1. Permeability to Ethanol of Porous HDPE Films Prepared via Drawing in the SC-CO_2 at Different Relative Deformations

ε (%)	W (vol %)	G (L/(h m^2))	d_{pore} [a] (nm)
80	17.4	0.1	
110	25.4	0.4	
220	30.1	4.0	7.4
250	30.0	3.9	7.7
300	24.2	6.7	9.4

[a]Using the Poiseuille equation.

Considering the pores in the HDPE film as the open-ended cylindrical channels perpendicular to the film surface and using the Poiseuille law, we calculated the average pores diameter (Table 1). Because the pores in the film stretched to 200% were characterized by a low interconnectivity and the true path length of the channels could not be estimated, the calculation of pore diameter was performed for the samples with the tensile strain of 220−300%. In that range of the relative deformation, the pores diameter was not significantly changed, being of 7−9 nm.

The prepared nanoporous polymeric films exhibited a good vapor permeability. For example, Figure 8 shows the evolution of relative humidity in the cell (cf. Figure 2) when using different polymeric films as the separator. It was found that the relative humidity developed after 10−15 min over the porous film (relative deformation 140% in SC-CO_2; Figure 8, curve 1) reached 70−80%. For comparison, the relative humidity developed in the same cell over the initial HDPE film or the film deformed in air to the tensile strain of 100−180% corresponding to the neck formation did not exceed 45% (Figure 8, curve 2).

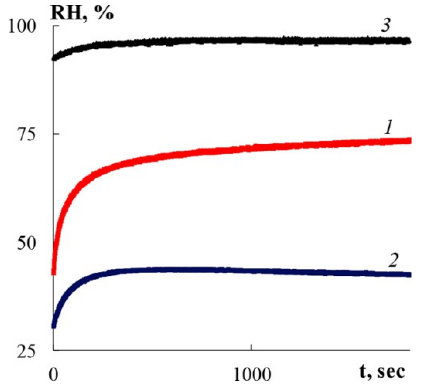

Figure 8. Kinetics of the change in relative humidity at 25 °C in the measuring cell over the HDPE films deformed in SC-CO_2 by 140% (1) and in air by 100% (2); the reference experiment using the same cell without any separator (3).

SAXS is among the most informative methods to investigate the materials containing pores with size 1−100 nm. For example,[53] SAXS has been successfully used in the study of crazes structure in porous glassy or partially crystalline polymeric materials. Figure 9 displays the 2D SAXS patterns and the corresponding curves of the scattering intensity in the equatorial direction for the HDPE films deformed in the SC-CO_2 by 100% (1) and 150%.

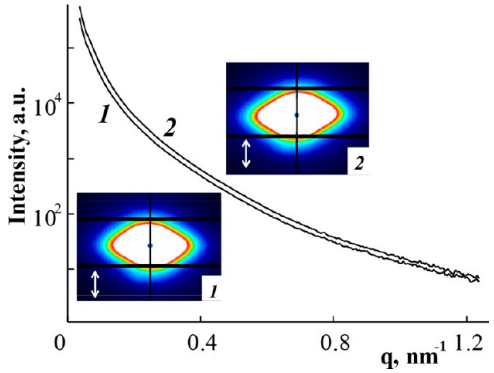

Figure 9. 2D SAXS patterns and the corresponding curves of the scattering intensity in the equatorial direction for the HDPE films deformed in the SC-CO_2 by 100% (1) and 150%.

and the corresponding curves of the scattering intensity in the equatorial direction for the films deformed in the supercritical fluid. The formation of the porous structure resulted in sharp (by several orders of magnitude) increase in the X-ray scattering intensity in comparison with the initial polymer. The shape of the scattering pattern after the film deformation in the SC-CO_2 was significantly changed, turning into a rhomb stretched along the equator and revealing two types of the scattering. The appearance of strong almost isotropic pattern localized at the q range below 0.6−0.7 nm^{-1} was evidently caused by the scattering from the walls of the crazes formed during the deformation. The weaker anisotropic pattern stretched along the equator was caused by the scattering on a system of the fibrils oriented parallel to the deformation direction and spanning the opposite walls of the crazes. Profiles of the intensity of the X-ray scattering in the equatorial direction (Figure 9) were diffuse, likely evidencing the absence of strictly ordered fibrillar-porous structure in the crazes and the existence of certain distribution of the distances between the fibril centers.

DOI: 10.1021/acs.macromol.7b02177
Macromolecules XXXX, XXX, XXX−XXX

Equatorial scattering curves can be routinely used for the calculation of fibrils diameter. It should be taken into account that this scattering is a superposition of that from crazes (the meridional component) and the fibrils (the equatorial component). To estimate the structural parameters of the fibrils filling the crazes, the meridional component was subtracted from the total equatorial scattering profile, and the obtained differential curve was processed as described elsewhere.[46] The calculations revealed that the HDPE fibrils were 10−12 nm in diameter, irrespective of the tensile strain.

To confirm that the drawing of the weakly structured HDPE film in the SC-CO_2 occurred via the crazing mechanism (resulting in the formation of the fibrillar-porous structure) and to visualize the structure development, we studied the polymeric samples by means of SEM. The microscopy images of the fractured HDPE film deformed in the SC-CO_2 by 100% are given in Figure 10. It is clearly seen that the drawing was

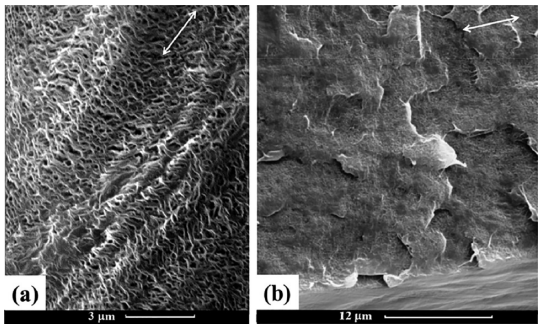

Figure 10. SEM images of the surface (a) and the cleavage (b) of the HDPE film deformed in the SC-CO_2 by 100%.

indeed accompanied by spatial separation of the lamellae or their stacks, resulting in the formation of the porous structure. The deformation of micrometer-scale level occurs strongly nonuniform at the initial stages: the areas with the spreading of majority of the lamellae coexisted with the parts not involved in the structural changes. The increase in the tensile strain led to steady decrease in the fraction of the nondeformed parts of the material. It should be noted that the microscopy images of the fractured samples did not revealed any porous (for example, cellular ones). The obtained image was similar to those usually observed for the HDPE film drawn in liquid AAM via the so-called delocalized (interlamellar) crazing mechanism.[22,54]

The SEM method is significantly limited in the study of the porous materials like the considered ones. The structure formed via crazing is relatively labile and unstable and can be strongly changed in response to the external factors such as high vacuum, thermal treatment, and so forth. Since the studied polymers were not conductive, their surface should be covered with a thin metal layer (for example, via spraying) prior to the SEM observation. Such sample preparation could significantly change the structure of the porous specimens.

In this study, the structural changes accompanying the uniaxial deformation of the HDPE films in the SC-CO_2 were visualized by means of AFM. This method has been earlier successfully used in the study of the development of the structure of polymer materials during the uniaxial deformation in liquid AAM[24] and for hard elastics.[55] Figure 11 shows the AFM images of the HDPE film surface after its drawing in the SC-CO_2 along the machine direction to different relative elongations. It is to be seen that the morphology of the deformed polymer surface was significantly changed in comparison with the initial film (Figure 3) or the film drawn in air at pressure of 0.1 MPa (Figure 5). When the tensile strain was up to 100%, a considerable fraction of the lamellae were twisted by 40°−50° to form the parquet pattern, likely via the shear mechanism. Only a relatively small part of the lamellae stacks was spread, forming a system of isolated fibrils oriented along the drawing direction. In other words, the crazing indeed occurred via the delocalized (interlamellar) mechanism. The diameter of the fibrils was close to the spacing between then (that is, the pores width). The increase in the tensile strain to 200% resulted in the steady growth of the amount of the crazes per a unit area, involving the entire specimen surface. That was accompanied by the fibrils elongation. Moreover, fractured

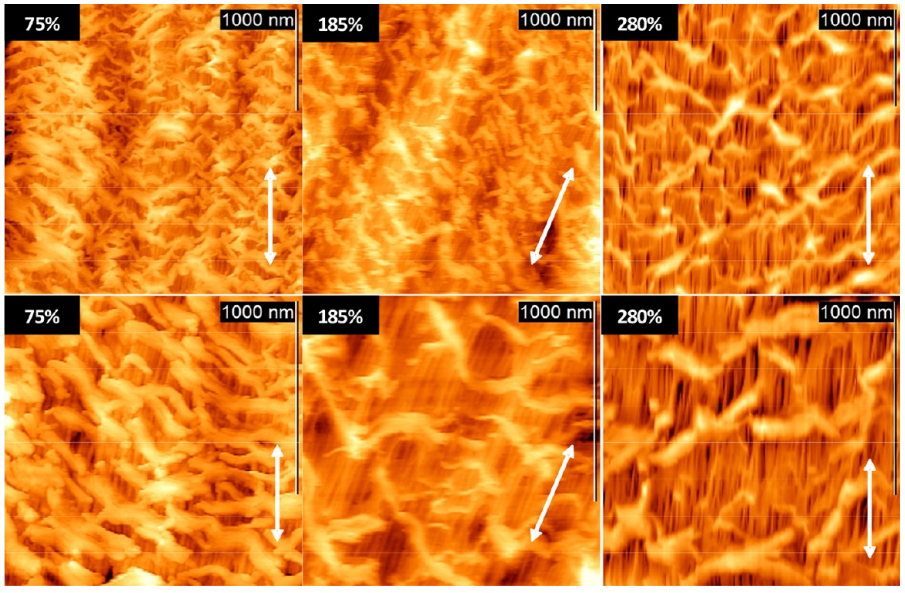

Figure 11. AFM images −3 × 3 μm (top) and 1.5 × 1.5 μm (bottom) of the HDPE film surface after the drawing in the SC-CO_2 along the machine direction. The machine direction is marked by arrows, and the tensile strain is indicated in the captions.

DOI: 10.1021/acs.macromol.7b02177
Macromolecules XXXX, XXX, XXX−XXX

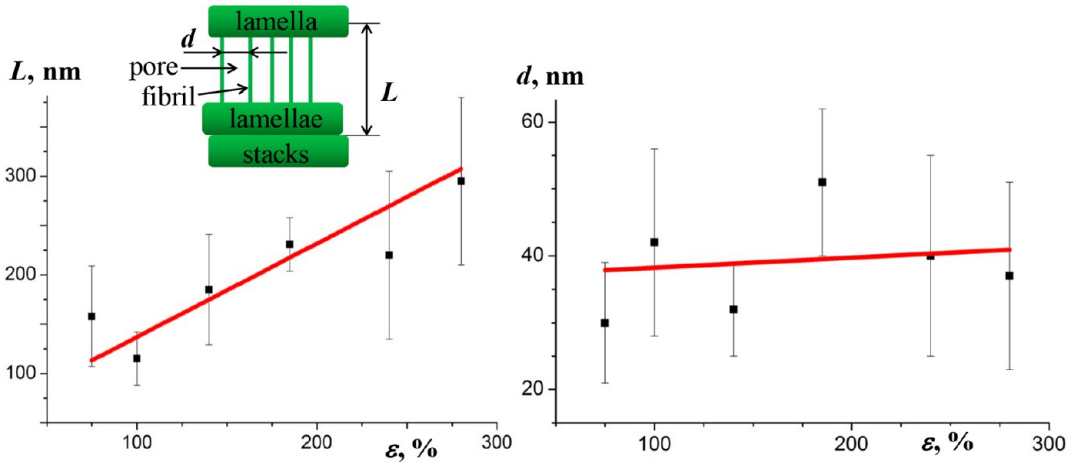

Figure 12. Average distance between the centers of the lamellae stacks L and average distance between the centers of fibrils in the direction perpendicular to the drawing d as functions of the tensile strain. The inset schematically illustrates the parameters L and d for the deformed samples.

lamellae appeared, their fraction also increasing with the increase in the draw ratio. At a high tensile strain (250−300%) practically all the lamellae were spread, significant part of the polymer material was transformed into the oriented fibrils, and the crazes were uniformly arranged over the surface of the deformed HDPE film. Furthermore, at a high tensile strain, a significant fraction of the lamella are fractured. At the same time, the polymer film did not collapse and retains the porous structure up to high draw ratios (300−400%) that is typical for the delocalized crazing.[20,22] In this case, the fibrils are formed between the lamellae, and their length does not exceed 200 nm. Such relatively short and stressed rods cannot be involved in significant thermal movement to form coagulation contacts, and the fibrils cannot be agglomerated to induce collapse of the porous structure.

Using the methods of mathematical processing and analysis of the AFM images, we obtained quantitative parameters describing the process of the polymeric film deformation in the supercritical fluid (Figure 12). The inset in the figure explains the parameters' meanings: L is the average distance between the centers of the lamellae stacks corresponding to the long period, and d is the average spacing between the fibrils centers in the transverse direction. Unfortunately, the fibril's diameter and the void's width could not be reliably determined from the obtained AFM images. The radius of curvature of the cantilever was 10 nm, and measurement of the structural elements comparable in the size was incorrect. However, the distance between the fibrils' tops was independent of the cantilever radius of curvature, and the sum of the diameter of the fibrils and the width of the pores between them could be measured with sufficient accuracy.

The presented plots show that the distance between the lamellae stacks grew with the increase in the tensile strain (from 90 nm for the initial film to 295 nm at the draw ratio of 280%). However, the thickness of the lamella stack is on average 45−60 nm at any tensile strain. Taking into account the SAXS data (Figure 3), we can assume that each stack consists of about 2−3 lamellae. These facts evidenced that a length of fibrils increased during drawing. But the average distance between the fibrils centers was only slightly changed, being of 30−40 nm. The relatively high variation of the L and d values (cf. the error bars in Figure 12) is remarkable. It could evidence the nonuniform deformation process (resulting in the irregular structure formed). That observation was confirmed by the diffuse SAXS patterns (Figure 9) in the meridional (reflecting the long period) and the equatorial (reflecting the distance between the fibrils centers) directions.

In summary, uniaxial deformation of extruded HDPE film in the SC-CO_2 occurred predominantly via the crazing mechanism, resulting in the formation of the high-disperse fibrillar-porous structure, the development of which was visualized by means of AFM. The obtained porous films contained a system of open interpenetrating nanometer-scale pores in the shape of slits, appearing due to the formation of isolated fibrils in the intercrystallite space during the lamellae spreading. A similar mechanism of the pores formation has been observed earlier during drawing of polyolefins in the presence of liquid AAM. That could evidence the generality of the polymer deformation mechanism in SC-CO_2 and in liquid AAM.

3.3. Reversibility of HDPE Deformation in SC-CO_2 Fluid. One of the remarkable features of the materials deformed via the crazing mechanism is the instability of their structure due to high reversibility of the deformations after the specimen unloading. Figure 13 shows the relative longitudinal shrinkage of the HDPE films drawn in the SC-CO_2 and in air.

Indeed, the polymeric films deformed in the supercritical fluid exhibited significant longitudinal shrinkage (up to 80%); that is practically recovery of the initial dimensions after unloading. On the contrary, the specimens deformed via the neck formation were shrunk by no more than 60%. The increase in the draw ratio resulted in the steady decrease in the

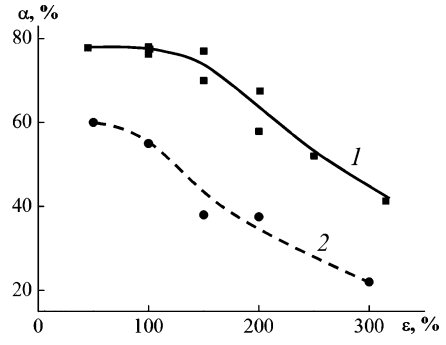

Figure 13. Relative longitudinal shrinkage of the HDPE films after drawing in SC-CO_2 (1) and in air (2) at 35 °C as functions of the tensile strain.

DOI: 10.1021/acs.macromol.7b02177
Macromolecules XXXX, XXX, XXX−XXX

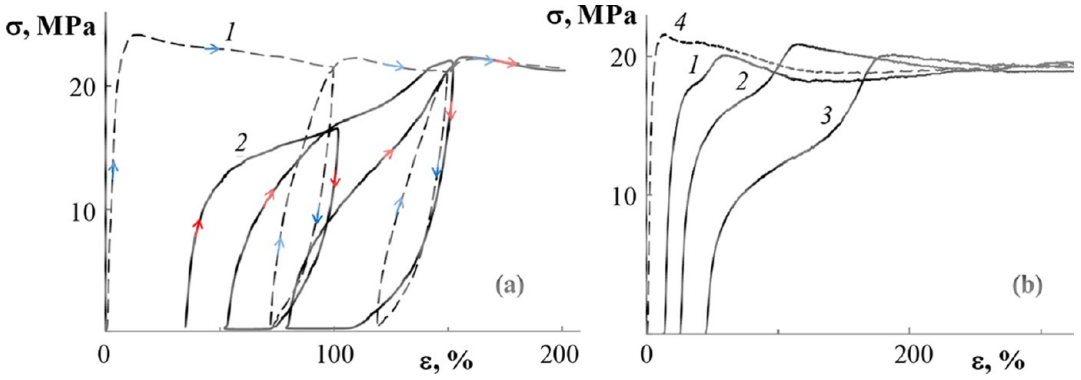

Figure 14. (a) Stress–strain curves of the initial HDPE film (1) and of the same film after drawing in CO_2 at 10 MPa/35 °C to 150% followed by shrinkage (2) during cyclic tensile mode at the room conditions; (b) Stress–strain curves of the HDPE specimens, preliminary stretched in CO_2 at 10 MPa/35 °C by 60% (1), 100% (2), and 150% (3) and shrunk in the same medium and of the initial HDPE film (4). All curves were recorded at the room conditions.

relative shrinkage (to 50% in the case of the drawing in SC-CO_2 and to 20% in the case of the drawing in air). That was evidently caused by the growing contribution of the irreversible shear deformation at higher tensile strain. The shrinkage was accompanied by the decrease in the specimen porosity (cf. curve 2 in Figure 6). Residual bulk porosity did not exceed 5–10% at the lower initial drawing ratio (up to 150%), reaching 20% at higher tensile strain (up to ε of 300%).

Formation of the crazes during the drawing in the SC-CO_2 imparted the HDPE material with mechanical properties unusual for the crystalline polymers. The differences in the mechanical behavior of the HDPE film before (dashed line) and after its uniaxial stretching in the SC-CO_2 followed by unloading are clearly seen in the stress–strain curves (Figure 14). The curves corresponding to the repeated measurements were shifted along the horizontal axis by the residual deformation value.

As was mentioned above, drawing of the film at 0.1 MPa in air was accompanied by the neck formation. In that case, when the yield stress was reached, part of the specimen was sharply narrowed (the neck was formed), and the cross-section area of the specimen was noticeably decreased. Further deformation occurred via the flow of the polymer material into the neck, reflected in the appearance of the plateau in the stress–strain curve. As was shown in the AFM images in the Figure 5, the main contribution to the deformation under these conditions is the irreversible shear mechanism. So unloading of the polymer deformed by necking resulted in its slight shrinkage (up to 20%). Repeated stretching led to rapid increase in the stress, and the curve exhibited a plateau in the same range of the relative deformation (cf. curve 1 in Figure 14a and cf. curve 4 in Figure 14b).

The shape of the stress–strain curve for the HDPE film deformed in the SC-CO_2 via the crazing mechanism and unloaded in the same medium was significantly different (Figure 14a, curve 2). In detail, the film stretching up to the value of the prior tensile strain (150% in the discussed case) occurred uniformly, without the gage narrowing. The specimen simultaneously turned milky-white again and was readily colored with an alcoholic solution of the dye. The marked features evidenced the recovery of the porous crazes structure (apparently, the structure was similar to that shown in Figure 11) collapsed during the shrinkage. Those repeatedly deformed specimens typically revealed high relative shrinkage values exceeding 50% in the cycling loading–unloading experiments. When the relative elongation in air ε exceeded the value of the prior tensile strain in SC-CO_2, the stress–strain curve 2 (Figure 14a) followed that for the initial film.

Let us comment on a distinctive feature of the stress–strain curves recorded during repeated stretching of the specimens deformed and shrunk in the SC-CO_2. Figure 14b displays such curves for the polymeric films differing in the tensile strain. The corresponding curves contained two steps. The first one was observed at low strains. It has been suggested[20] that the first stage corresponds to the opening of the crazes and recovery of the fibrillar-porous structure. The second step appeared at the relative deformation corresponding to the prior tensile strain of the film in the SC-CO_2, and the repeatedly recorded curve followed that for the initial HDPE film. Similar curves have been earlier obtained[20] during repeated stretching of amorphous and partially crystalline polymers stretched in liquid media via the crazing mechanism and dried in the unloaded state.

We examined the structure of the shrunk films. Figure 15 shows the 2D SAXS pattern and the AFM image of the specimen deformed and unloaded in the supercritical fluid.

It is to be seen that the oriented fibrillar structure disappeared during the shrinkage. In detail, the anisotropic reflection on the equator (usually assigned to the scattering on a system of separated ordered fibrils) disappeared in the SAXS pattern, and the scattering turned almost isotropic, somewhat

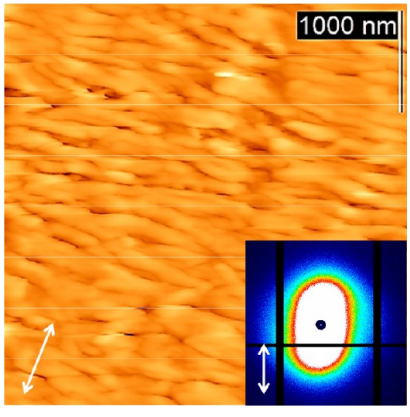

Figure 15. AFM image of the sample after its drawing by 150% and shrinkage in SC-CO_2. The inset shows the 2D SAXS pattern of the shrunk specimen. The arrow marks the drawing (shrinkage) direction.

DOI: 10.1021/acs.macromol.7b02177
Macromolecules XXXX, XXX, XXX–XXX

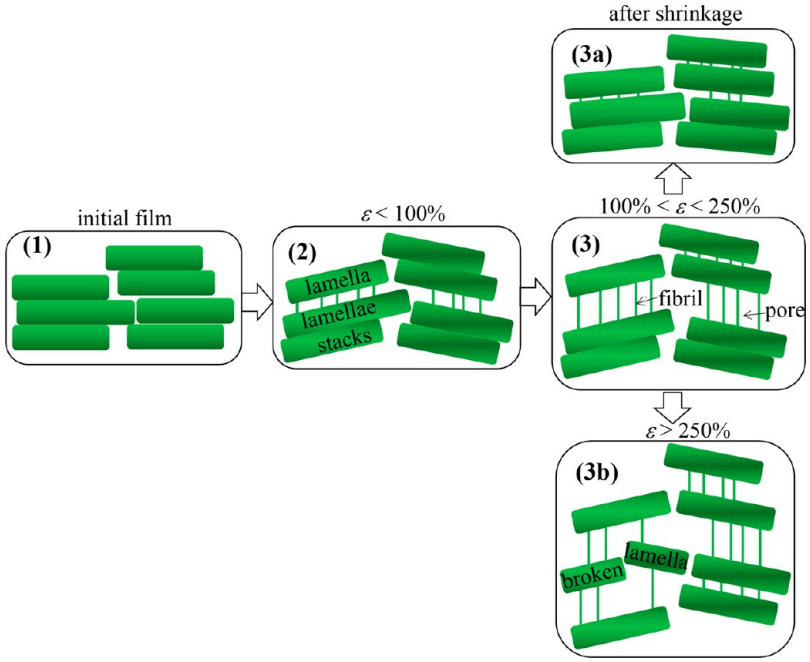

Figure 16. Scheme of the development of a porous structure of HDPE film during uniaxial stretching in the presence of SC-CO_2 and after shrinkage.

elongated in the meridional direction. At the same time, the AFM image revealed the formation of fairly regular folded structure, with the about 100 nm thick folds (average spacing between the fold centers 190 nm) were oriented perpendicular to the drawing-shrinkage direction. It can be speculated that such structure could be formed via closing of the crazes and reapproaching of the lamellae (the long period was down almost to the value typical of the initial HDPE film). The mechanism of such high reversible deformations has remained unclear so far. It has been suggested[56] that the driving force of the shrinkage is the entropic elasticity, mainly the excessive surface free energy and high specific surface area of the crazes. After the shrinkage, more compliant material was concentrated between the lamellae, and it could be readily deformed at relatively low stress during initial stage of the repeated stretching (Figure 14), thus restoring the initial fibrillar-porous crazed structure. Hence, uniaxial drawing of the HDPE film along the machine direction in the SC-CO_2 followed by shrinkage is an approach to produce the "half-finished" material, its stretching in air under ambient conditions affording the open-porous membranes.

4. CONCLUSIONS

In this study, the process of formation of open-porous structure during uniaxial stretching of the HDPE film in the SC-CO_2 was described and visualized by means of AFM. It was demonstrated that the supercritical fluid acted as the AAM, and the formation of the porous structure occurred via the crazing mechanism due to spreading of the lamellae and the appearance of a system of isolated ordered nanometer-scale fibrils in the interlamellar space. The width of the slitlike pores and the fibril's diameter were about 10 nm. The obtained nanoporous films exhibited good liquid and vapor permeability.

According to the structural and mechanical methods, a scheme of the development of a porous structure of HDPE film during uniaxial stretching in the presence of supercritical fluid and after shrinkage is presented in Figure 16. At the first stage (section 2), the stacks of lamellas bend and form parquet structure, and then they separate over along the machine direction. As a result, fibrillar-porous structure is formed between them. With a growth of the tensile strain (section 3), the distance between stacks increase due to the elongation of fibrils. At a high tensile strain (section 3b), lamellas inside the stacks are separated and broken.

Reversibility of large deformations of the HDPE in the SC-CO_2 and the feature of mechanical behavior of the shrunk samples were studied. It was demonstrated that the longitudinal shrinkage of the polymeric film (reaching 80%) was accompanied by approximation of the lamellae and disappearance of the oriented fibrillar structure (Figure 16, section 3a). The shrunk films exhibited the properties of hard-elastic materials, and their repeated stretching in air at room conditions led to the restoration of the open-porous structure.

Since the crazing in the presence of AAM is a fundamental phenomenon typical of majority of glassy and partially crystalline polymers, it is reasonable to expect that the described approach can serve as a universal approach for the preparation of membranes with open nanoporous structure based on many polymers including industrial ones. The use of supercritical CO_2 as the AAM makes the process environmentally friendly.

AUTHOR INFORMATION

Corresponding Author

*E-mail dudnik@physics.msu.ru (A.O.D.).

ORCID

Anna O. Dudnik: 0000-0001-7425-591X
Elena S. Trofimchuk: 0000-0002-8035-7872
Ekaterina G. Rukhlya: 0000-0001-5506-654X

Notes

The authors declare no competing financial interest.

ACKNOWLEDGMENTS

This study was financially supported by the Russian Science Foundation (project no. 17-13-01017). This work was done

DOI: 10.1021/acs.macromol.7b02177
Macromolecules XXXX, XXX, XXX−XXX

using the equipment provided by the M.V. Lomonosov Moscow State University Program of Development. X-ray measurements has been performed at the unique scientific facility of the Kurchatov Synchrotron Radiation Source supported by the Ministry of Education and Science of the Russian Federation (project no. RFMEFI61917X0007). Authors are grateful to Dr. A. Gruzinov for the assistance in the SAXS experiments, to Dr. A.A. Dolgova for the help with conducting the pressure gradient permeability test, to Dr. D.V. Bagrov for the assistance with the AFM measurements, and to G. Armeev for the development of the vapor permeability cell.

REFERENCES

(1) Liu, Y.; Wang, G. In *Nanostructured Polymer Membranes: Applications, Membranes: Technology and Applications*; Visakh, P. M., Nazarenko, O., Eds.; John Wiley& Sons, Inc.: Hoboken, NJ, 2016; Vol. 2, pp 27−88.
(2) Le, N. L.; Nunes, S. P. Materials and Membrane Technologies for Water and Energy Sustainability. *Sustainable Mater. Technol.* **2016**, *7*, 1−28.
(3) Trofimchuk, E. S.; Nikonorova, N. I.; Chagarovskii, A. O.; Volynskii, A. L.; Bakeev, N. F. Crystallization of Silver Chloride in Crazed Porous Polymers. *J. Phys. Chem. B* **2005**, *109*, 16278−16283.
(4) Ma, J.; Yang, Z.; Wang, X.; Qu, X.; Liu, J.; Lu, Y.; Hu, Z.; Yang, Z. Flexible Bi-Continuous Mesostructured Inorganic/Polymer Composite Membranes. *Polymer* **2007**, *48*, 4305−4310.
(5) Okkelman, I. A.; Dolgova, A. A.; Banerjee, S.; Kerry, J. P.; Volynskii, A.; Arzhakova, O. V.; Papkovsky, D. B. Phosphorescent Oxygen and Mechanosensitive Nanostructured Materials Based on Hard Elastic Polypropylene Films. *ACS Appl. Mater. Interfaces* **2017**, *9*, 13587−13592.
(6) Caruso, R. A.; Antonietti, M. Silica films with bimodal pore structure prepared by using membranes as templates and amphiphiles as porogens. *Adv. Funct. Mater.* **2002**, *12*, 307−312.
(7) Trofimchuk, E. S.; Nikonorova, N. I.; Nesterova, E. A.; Yakukhnov, S. A.; Mal'tsev, D. K.; Inozemtseva, M. N.; Volynskii, A. L.; Bakeev, N. F. Obtaining Nanoporous Inorganic Sheets. *Nanotechnol. Russ.* **2012**, *7*, 352−358.
(8) Mulder, M. *Basic Principles of Membrane Technology*; Kluwer Academic Publishers: Dordrecht, 1996.
(9) Chen, S.; Nandi, S.; Winter, H. H.; Gido, S. P. Oriented Lamellar Structure and Pore Formation Mechanism in CSX-Processed Porous High-Density Polyethylene. *Macromolecules* **2006**, *39*, 2849−2855.
(10) Wu, D.; Xu, F.; Sun, B.; Fu, R.; He, H.; Matyjaszewski, K. Design and Preparation of Porous Polymers. *Chem. Rev.* **2012**, *112*, 3959−4015.
(11) Trifkovic, M.; Hedegaard, A.; Huston, K.; Sheikhzadeh, M.; Macosko, C. W. Porous Films via PE/PEO Cocontinuous Blends. *Macromolecules* **2012**, *45*, 6036−6044.
(12) Zhang, Y.; Ionov, L. Actuating Porous Polyimide Films. *ACS Appl. Mater. Interfaces* **2014**, *6*, 10072−10077.
(13) Matsuyama, H.; Okafuji, H.; Maki, T.; Teramoto, M.; Kubota, N. Preparation of Polyethylene Hollow Fiber Membrane Viathermally Induced Phase Separation. *J. Membr. Sci.* **2003**, *223*, 119−126.
(14) Kravets, L. I.; Dmitriev, S. N.; Apel, P. Y. Production and Properties of Polypropylene Trackmembranes. *Collect. Czech. Chem. Commun.* **1997**, *62*, 752−760.
(15) Pawlak, A.; Galeski, A.; Rozanski, A. Cavitation During Deformation of Semicrystalline Polymers. *Prog. Polym. Sci.* **2014**, *39*, 921−958.
(16) Novikov, D.; Elyashevich, G.; Lavrentyev, V.; Kuryndin, I.; Saprykina, N.; Vorobyev, G.; Varlamov, A.; Bukošek, V. Superlattices of Lamellae in Microporous Oriented Polyolefin Films. *Phys. Solid State* **2013**, *55*, 443.
(17) Li, X.; Meng, L.; Lin, Y.; Chen, X.; Zhang, Q.; Zhang, R.; Wu, L.; Zhang, W.; Li, L. Preparation of Highly Oriented Polyethylene-Precursor Film with Fibril and Its Influence on Microporous Membrane Formation. *Macromol. Chem. Phys.* **2016**, *217*, 974−986.
(18) *Nano- and Micromechanics of Polymers and Composites*; Karger-Kocsis, J., Fakirov, S., Eds.; Hanser Publisher: Munich, 2009; p 604.
(19) Ren, Ch.; Jiang, Zh.; Du, X.; Men, Yo.; Tang, T. Microstructure and Deformation Behavior of Polyethylene/Montmorillonite Nanocomposites with Strong Interfacial Interaction. *J. Phys. Chem. B* **2009**, *113*, 14118−14127.
(20) Volynskii, A. L.; Bakeev, N. F. *Solvent Crazing of Polymers*; Elsevier: Amsterdam, 1995; p 413.
(21) *Definitions of Terms Relating to Degradation, Aging, and Related Chemical Transformations of Polymers* (IUPAC Recommendations 1996); Hatada, K.; Fox, R. B.; Kahovec, J.; Marechal, E.; Mita, I.; Shibaev, V., Eds. *Pure Appl. Chem.* 1996, *68*, pp 2317, https://iupac.org/publications/pac/1996/pdf/6812x2313.pdf.
(22) Yarysheva, A. Y.; Rukhlya, E. G.; Yarysheva, L. M.; Bagrov, D. V.; Volynskii, A. L.; Bakeev, N. F. The Structural Evolution of High-Density Polyethylene During Crazing in Liquid Medium. *Eur. Polym. J.* **2015**, *66*, 458−469.
(23) Robeson, L. M. Environmental Stress Cracking: A Review. *Polym. Eng. Sci.* **2013**, *53*, 453−467.
(24) Bagrov, D. V.; Yarysheva, A. Y.; Rukhlya, E. G.; Yarysheva, L. M.; Volynskii, A. L.; Bakeev, N. F. Atomic Force Microscopic Study of the Structure of High-Density Polyethylene Deformed in Liquid Medium by Crazing Mechanism. *J. Microsc.* **2014**, *253*, 151−160.
(25) Sinevich, E. A.; Prazdnichnyi, A. M.; Bakeev, N. F. Structural Rearrangements in Crazed Polymers Induced by Sublimation Drying. *Vysokomol. Soedin., Ser. A* **1995**, *37*, 1521−1527.
(26) Arzhakova, O. V.; Dolgova, A. A.; Yarysheva, L. M.; Volynskii, A. L.; Bakeev, N. F. Development of a Stable Open-Porous Structure in the Solvent-Crazed High-Density Polyethylene. *Inorg. Mater.* **2011**, *2*, 493−498.
(27) Olf, H. G.; Peterlin, A. Crazing and Fracture in Crystalline, Isotactic Polypropylene and the Effect of Morphology, Gaseous Environments, and Temperature. *J. Polym. Sci., Polym. Phys. Ed.* **1974**, *12*, 2209−2251.
(28) Brown, N.; Metzger, B. D. The Dependence of Craze Velocity on the Pressure and Temperature of the Environmental Gas. *J. Polym. Sci., Polym. Phys. Ed.* **1980**, *18*, 1979−1992.
(29) Volynskii, A. L.; Yarysheva, L. M.; Ukolova, Ye. M.; Kozlova, O. V.; Vagina, T. M.; Kechek'yan, A. S.; Kozlov, P. V.; Bakeyev, N. F. On the Two Mechanisms of the Effect of Physically Aggressive Media on the Mechanical Properties and Structure of Polyamide-6. *Polym. Sci. U. S. S. R.* **1987**, *29*, 2877−2883.
(30) *Supercritical Fluids: Fundamentals and Applications*; Kiran, E., Debenedetti, P. G., Peters, Kluwer, C. J., Eds.; Springer: Dordrecht, Netherlands, 2000; p 596.
(31) Kazarian, S. G. Polymer Processing with Supercritical Fluids. *Polym. Sci., Ser. C* **2000**, *42*, 78−101.
(32) King, J. W.; Srinivas, K. Multiple Unit Processing Using Sub- and Supercritical Fluids. *J. Supercrit. Fluids* **2009**, *47*, 598−610.
(33) Kiran, E. Supercritical Fluids and Polymers - The Year in Review − 2014. *J. Supercrit. Fluids* **2016**, *110*, 126−153.
(34) Siripurapu, S.; Coughlan, J. A.; Spontak, R. J.; Khan, S. A. Surface-Constrained Foaming of Polymer Thin Films with Supercritical Carbon Dioxide. *Macromolecules* **2004**, *37*, 9872−9879.
(35) Guo, H.; Nicolae, A.; Kumar, V. Solid-State Poly(methyl methacrylate) (PMMA) Nanofoams. Part II: Low-Temperature Solid-State Process Space Using CO_2 and the Resulting Morphologies. *Polymer* **2015**, *70*, 231−241.
(36) Tsivintzelis, I.; Angelopoulou, A. G.; Panayiotou, C. Foaming of Polymers with Supercritical CO_2: An Experimental and Theoretical Study. *Polymer* **2007**, *48*, 5928−5939.
(37) Bao, J.-B.; Liu, T.; Zhao, L.; Hu, G.-H.; Miao, X.; Li, X. Oriented Foaming of Polystyrene with Supercritical Carbon Dioxide for Toughening. *Polymer* **2012**, *53*, 5982−5993.
(38) Ma, Z.; Zhang, G.; Yang, Q.; Shi, X.; Shi, A. Fabrication of Microcellular Polycarbonate Foamswith Unimodal or Biomodal Cell Size Distributions Using Supercritical Carbon Dioxide as a Blowing Agent. *J. Cell. Plast.* **2014**, *50*, 55−79.

DOI: 10.1021/acs.macromol.7b02177
Macromolecules XXXX, XXX, XXX−XXX

(39) Jiang, X.-L.; Liu, T.; Xu, Zh.-M.; Zhao, L.; Hu, G.-H.; Yuan, W.-K. Effects of Crystal Structure on the Foaming of Isotactic Polypropylene Using Supercritical Carbon Dioxide as a Foaming Agent. *J. Supercrit. Fluids* **2009**, *48*, 167−175.
(40) Li, D-Ch.; Liu, T.; Zhao, L.; Yuan, W.-K. Foaming Of Linear Isotactic Polypropylene Based on Its Non-Isothermal Crystallization Behaviors Under Compressed CO_2. *J. Supercrit. Fluids* **2011**, *60*, 89−97.
(41) Xing, Z.; Wu, G.; Huang, S.; Chen, S.; Zeng, H. Preparation of Microcellular Cross-Linked Polyethylene Foams by a Radiation and Supercritical Carbon Dioxide Approach. *J. Supercrit. Fluids* **2008**, *47*, 281−289.
(42) Nofar, M.; Park, C. B. Poly(lactic acid) Foaming. *Prog. Polym. Sci.* **2014**, *39*, 1721−1741.
(43) Hu, X.; Lessery, A. J. Solid-State Processing of Polymer in the Presence of Supercritical Carbon Dioxide. *J. Cell. Plast.* **2006**, *42*, 517−527.
(44) Geng, L.; Li, L.; Mi, H.; Chen, B.; Sharma, P.; Ma, H.; Hsiao, B. S.; Peng, X.; Kuang, T. Superior Impact Toughness and Excellent Storage Modulus of Poly(lactic acid) Foams Reinforced by Shish-Kebab Nanoporous Structure. *ACS Appl. Mater. Interfaces* **2017**, *9*, 21071−21076.
(45) Trofimchuk, E. S.; Efimov, A. V.; Nikitin, L. N.; Nikonorova, N. I.; Dolgova, A. A.; Yarysheva, L. M.; Arzhakova, O. V.; Volynskii, A. L.; Bakeev, N. F.; Khokhlov, A. R. Crazing of Polymers in a Supercritical Carbon Dioxide Fluid. *Dokl. Chem.* **2009**, *428*, 238−241.
(46) Trofimchuk, E. S.; Efimov, A. V.; Nikonorova, N. I.; Volynskii, A. L.; Bakeev, N. F.; Nikitin, L. N.; Khokhlov, A. R.; Ozerina, L. A. Crazing of Isotactic Polypropylene in the Medium of Supercritical Carbon Dioxide. *Polym. Sci., Ser. A* **2011**, *53*, 546−557.
(47) Osaka, N.; Kono, F.; Saito, H. SAXS Study on Deformation Behavior of Isotactic Polypropylene Under Pressurized CO_2. *J. Appl. Polym. Sci.* **2013**, *127*, 1228−1236.
(48) Yaminsky, Y.; Filonov, A.; Sinitsyna, O.; Meshkov, G. FemtoScan Online Software. *Nanoindustriya* **2016**, *2*, 42−46.
(49) Feijoo, J. L.; Sanchez, J. J.; Muller, A. J. The Phenomenon of Double Yielding in Blown Polyethylene Films. *Polym. Bull.* **1997**, *39*, 125−132.
(50) Prasad, A.; Shroff, R.; Rane, S.; Beaucage, G. Morphological Study of HDPE Blown Films by SAXS, SEM and TEM: A Relationship Between the Melt Elasticity Parameter and Lamellae Orientation. *Polymer* **2001**, *42*, 3103−3113.
(51) Zhang, X. M.; Elkoun, S.; Ajji, A.; Huneault, M. A. Oriented Structure and Anisotropy Properties of Polymer Blown Films: HDPE, LLDPE And LDPE. *Polymer* **2004**, *45*, 217−229.
(52) Murakami, S.; Kohjiya, S.; Shimamura, K. Comparative Study of Structure and Tensile Properties of Melt-Pressed and Extruded-Blown Films of High-Density Polyethylene. *J. Macromol. Sci., Part B: Phys.* **2000**, *39* (5−6), 645−655.
(53) Chu, B.; Hsiao, B. S. Small-Angle X-ray Scattering of Polymers. *Chem. Rev.* **2001**, *101*, 1727−1761.
(54) Yarysheva, A. Y.; Bagrov, D. V.; Bakirov, A. V.; Tarasevich, B. N.; Grohovskaya, T. E.; Yarysheva, L. M.; Chvalun, S. N.; Volynskii, A. L. Polyethylene−Poly(ethylene oxide) Hybrid Films Obtained by Crazing and Their Structural Peculiarities. *Macromolecules* **2017**, *50*, 2881−2888.
(55) Hild, S.; Gutmannsbauer, W.; Lüthi, R.; Fuhrmann, J.; Güntherodt, H.-J. A Nanoscopic View of Structure and Deformation of Hard Elastic Polypropylene with Scanning Force Microscopy. *J. Polym. Sci., Part B: Polym. Phys.* **1996**, *34*, 1953−1959.
(56) Volynskii, A. L.; Grokhovskaya, T. E.; Kulebyakina, A. I.; Bol'shakova, A. V.; Bakeev, N. F. Visualization of Structural Rearrangements During Annealing of Solvent-Crazed Isotactic Polypropylene. *Polym. Sci., Ser. A* **2009**, *51*, 396−406.

DOI: 10.1021/acs.macromol.7b02177
Macromolecules XXXX, XXX, XXX−XXX